Soft Matter

ARTICLE TYPE

Cite this: DOI: 00.0000/xxxxxxxxxx

Motility of acoustically powered micro-swimmers in a liquid crystalline environment

Jaideep Katuri, Alexey Snezhko, Andrey Sokolov*

Received Date
Accepted Date

DOI: 00.0000/xxxxxxxxxx

Suspensions of microswimmers in liquid crystals demonstrate remarkably complex dynamics and serve as a model system for studying active nematics. So far, experimental realization of microswimmers suspended in liquid crystalline media has relied on biological microorganisms that impose strict limitations on the compatible media and makes it difficult to regulate activity. Here, we demonstrate that acoustically powered bubble microswimmers can efficiently self-propel in a lyotropic liquid crystal. The velocity of the swimmers is controlled by the amplitude of the acoustic field. Histograms of swimming directions with respect to the local nematic field reveal a bimodal distribution: the swimmers tend to either fully align with or swim perpendicular to the director field of the liquid crystal, occasionally switching between these two states. The bubble-induced streaming from a swimmer locally melts the liquid crystal and produces topological defects at the tail of the swimmer. We show that the defect proliferation rate increases with the angle between the swimmer's velocity and the local orientation of the director field.

1 Introduction

Active matter systems are inherently out of equilibrium as their constituent particles continuously consume energy and convert it into mechanical motion[1–4]. A suspension of motile particles in a liquid can locally generate mechanical stresses and flows, giving rise to complex inter-particle and particle-medium interactions[5–7]. Active systems have however been overwhelmingly studied in isotropic Newtonian fluids where they possess direction independent physical properties, and the swimming activity does not significantly alter the fluid medium, aside from the locally generated flows. Liquid crystals, on the other hand, are anisotropic media that consist of molecules of different shapes (for example elongated, discoidal, or banana-shaped) with aligning interactions that preserve long-range orientational order. The orientational order leads to the physical properties of the medium, such as dielectric permittivity, electric conductivity, and viscosity to be anisotropic[8]. Dispersing colloidal particles into liquid crystals (LCs) promotes ordered particle assemblies induced from the orientational order of the medium, but can also introduce topological defects leading to a complex interplay between the particles and the host medium[9].

Active nematics (also termed as active liquid crystals) is a rapidly expanding class of out-of-equilibrium systems that combine the mechanical properties of liquid crystals with motility introduced on a microscopic level[10,11]. Motile particles introduce additional complexity due to the coupling between the swimming motion and the anisotropy in the medium. Examples of active nematics currently include microtubule (or actine)-motor protein mixtures[12,13], cellular nematics[14], and suspensions of bacterial swimmers in liquid crystalline media[15–20]. The use of biological swimmers poses several downsides: biological degradation of the system due to aging and nutrient consumption, the difficulty of controlling activity (swimmers velocity), and poor repeatability of the results due to variation of biological components between experiments. To overcome these issues artificial self-propelled particles should replace biological swimmers in LC media.

There are several challenges to developing systems of synthetic active particles suspended in LCs. Chemically powered swimmers which are driven through a self-diffusiophoretic mechanism[21] results in a chemical modification of the liquid crystal's composition which often alters or destroys the nematic order. Recently suggested topological defect assisted swimming of the magnetized particles in a rotational magnetic field enables new type of swimmers in which propulsion is generated by a complex swim strokes where attached topological defects periodically extend, depin, and contract[22]. However, the transnational velocity of such colloids is low (a fraction of the particle size per second) rendering them not appropriate for the task of injecting enough energy at the microscopic level to lead to a proliferation of activity induced topological defects - a hallmark of active nematic

Materials Science Division, Argonne National Laboratory, 9700 South Cass Avenue, Lemont, IL 60439, USA

† Electronic Supplementary Information (ESI) available: [details of any supplementary information available should be included here]. See DOI: 10.1039/cXsm00000x/

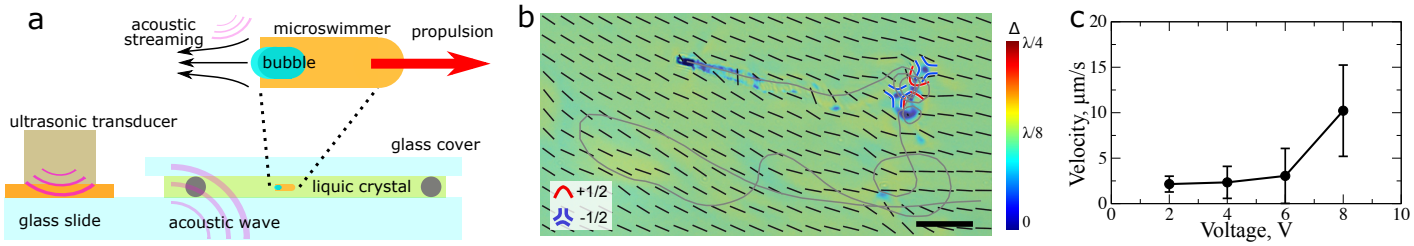

Fig. 1 (a) Schematics of the experimental setup. Microscopic swimmers are suspended in a drop of liquid crystal (DSCG) which is sandwiched between two glass slides. An ultrasound transducer is glued to the bottom glass slide. The propulsion of a bubble swimmer is enabled by the high-frequency oscillations of an air bubble and induced microstreaming of the fluid media. (b) Example of a swimming trajectory (gray line) in the liquid crystal. The local orientation of the nematic field is shown by short black lines. Color illustrates optical retardance Δ. Generated positive (+1/2) and negative (-1/2) topological defects are shown by red and blue symbols correspondingly. Also see Movie 1. The scale bar is 25 μm. (c) The average swimming speed of bubble swimmers as a function of the amplitude of the voltage applied to the transducer. The excitation frequency is linearly swept in the range 0.9-1.3 MHz each 50 ms.

systems.

In this paper we realize a system of active particles self-propelled via air bubble streaming mechanism[23–28] externally energized by an acoustic field. We demonstrate that the sound wave efficiently energizes the colloidal swimmers but has minimal effect on the nematic ordering of the liquid crystal. This allows us to create a fully synthetic system that combines active swimmers and anisotropic fluid medium. We find that these particles are efficient swimmers in the LC medium, capable of propulsion speeds up to several body lengths per second, respond to the local orientational order of the liquid crystal, and continuously generate topological defects in the medium with the defect proliferation rate increasing with the angle between the swimmer's velocity and the local orientation of the director field.

2 Results

In our experiments, we use hollow cylindrical microstructures as micro-swimmers, that are 3D printed via two-photon polymerization (Nanoscribe Photonic GT) of a polymer photoresist. The microstructures have one of their ends sealed to effectively encapsulate the bubble while the other end is open to allow for acoustic streaming in a fluid medium. The swimmers have a length of 15 μm and an inner radius of 2.5 μm and are produced in large batches (>20000 structures) on an ITO-coated silica substrate. The microstructures are then dispersed in the LC fluid medium (a 12 wt% solution of chromonic lyotropic LC material disodium cromoglycate (DSCG) is used). The concentration of the DSCG is chosen to obtain the nematic phase at room temperature with the lowest possible viscosity. The experimental chamber is composed of two silica glass slides separated by 8 μm spacers. An ultrasound transducer (1MHZ Unictron's LPY1 from Digi-Key) is glued to the bottom slide to produce an acoustic field (Fig. 1a). The setup spatially confines the swimmers in the vertical direction, forcing them to swim parallel to the confining substrates. Air bubbles are formed in most of the cylindrical microstructures immediately upon introduction into the LC medium due to the hydrophobic surface treatment of the particles.

We obtain image sequences from the experiments using a custom-built polarization microscope and a polarization monochrome camera (FLIR 3.1 Blackfly® S). The sample with the active swimmers suspended in LC is illuminated by monochrome circularly polarized light (570 nm). The polarization camera has a sensor consisting of 1124x1024 four-pixel (2x2) blocks. Each of these blocks, known as a calculation unit, is overlaid with a polarizer array comprising four different angled polarizers (0^0, 45^0, 90^0, and 135^0). Using this camera, the optical retardance, orientations of optical axes of a birefringent material, and then the director field in LC can be reconstructed locally by comparing the amplitudes of light intensities of each pixel in the calculation unit by using Jones or Mueller calculus[29] (see SI for an example of such reconstruction). Importantly, the explicit reconstruction of the order parameter is only possible for a sufficiently thin film with the thickness d satisfying $d\Delta n < \lambda/4$, where Δn is the local birefringence of LC and λ is the wavelength of the monochrome illuminating light. This technique allows us to visualize the changes in the local order parameter and the director field in the LC at a high frame rate.

A waveform generator (Agilent 33220a) powering an ultrasound transducer is used to apply an acoustic field signal to our system, see Fig. 1a. Immediately upon application of the acoustic field, the water-air interface of the bubble located at the tail of each swimmer starts to pulsate and generate microscopic streaming[25]. A propulsive force is generated in the opposite direction of the streaming and pushes the swimmer along its long axis, see Fig. 1b and Movie 1. The swimming speed can be externally manipulated by the amplitude of the applied signal, Fig 1c. The mechanism of self-propulsion of bubble swimmers and asymmetry of produced flow has been previously studied for swimmers in isotropic liquids[26,30,31]. Because of the asymmetric confinement of the air bubble by the 3D printed microstructure, a net cavitation microstream flows away or towards its open end depending on the location of the bubble in the microstructure[32] The temporal symmetry of the oscillatory flows generated by the air bubble is broken due to non-negligible fluid inertia of the flow produced by the bubble oscillations leading to a secondary flow (acoustic streaming) propelling the structure.

To our knowledge, no experimental or theoretical investigations have been conducted on the swimming dynamics of bubble swimmers in anisotropic viscoelastic mediums.

The propagation of a sound wave in LC medium is accompa-

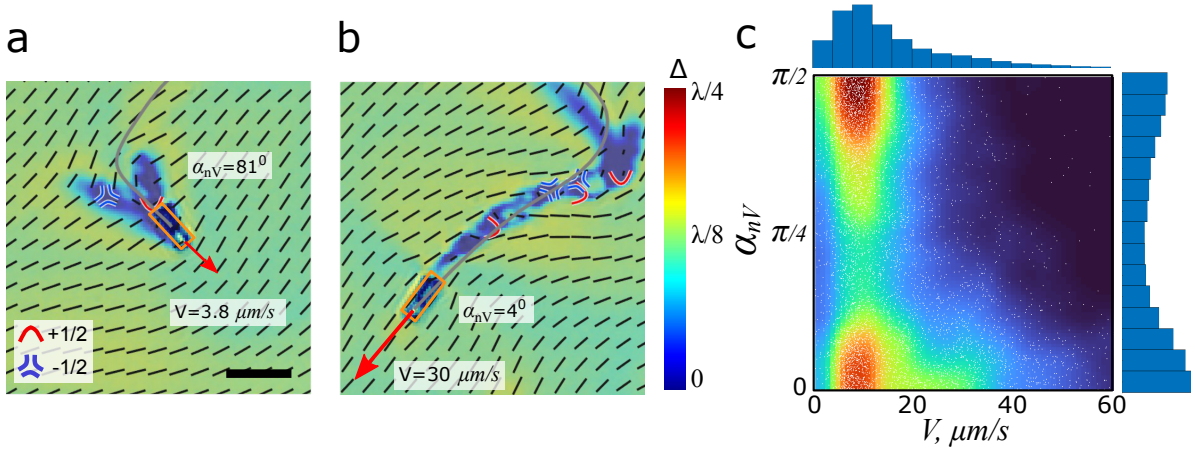

Fig. 2 Orientation of swimmers relative to the local nematic field. (a-b) Examples of a swimmer changing the swimmer direction from parallel to perpendicular (a) and vice versa (b). V is instantaneous swimming speed, and α_{nV} is the angle between velocity and local nematic field orientation. When the swimmer is moving perpendicular to the nematic field (a) swimming speed is significantly slower than during parallel swimming (b). Positive and negative topological defects are shown by red and blue symbols. Also, see Movie 2. The scale bar is 20 microns. (c) Two-dimensional probability distribution function of the angle between swimmer's velocity and local orientation of nematic field α_{nV} and swimming speeds V. Each white dot corresponds to a single measurement. The top and right barplots show 1D distributions of V and α_{nV} correspondingly. The applied voltage amplitude is $10V_{pp}$. The excitation frequency is linearly swept in the range 0.9-1.3 MHz each 50 ms.

nied by a wide plethora of physical phenomena - attenuation, scattering, dispersion of acoustic waves, as well as diffraction on topological defects[33–35]. Additionally, in contrast to water (or isotropic fluids) where sound propagates in the form of a longitudinal wave, the elasticity of LC enables the propagation of transverse waves with a different wavelength and phase speed. A pattern of standing and traveling acoustic waves in LC becomes increasingly complex and its detailed study is beyond the scope of this work. Using a single frequency (in the range of $0.5-1.5$ MHz) acoustic excitation field we observed that the activity of swimmers is not homogeneous over the field of view (roughly 1mm x 1mm) as a result of non-uniform wave patterns. The swimmer may suddenly stop propelling upon entering a "non-active" zone (see Movie 3) and then continue to swim after a small change in the driving frequency. The change in the driving frequency alters the shape of the acoustic pattern due to the corresponding change in the wavelength. To minimize the variations of swimming speeds over the field of view, we randomize the acoustic field pattern by rapidly sweeping the frequency of the applied driving frequency between $0.9-1.3$ MHz every 50 ms. Such a design of the signal homogenizes the swimming activity over the observation window.

2.1 Velocity dependence of the swimmers on the direction of the nematic field

Biological rod-shaped microswimmers, such as bacteria *E. Coli* or *B. Subtilis*, swim strongly anisotropically in an LC medium: the bacterial motion in the bulk is constrained along linear paths parallel to the local director field[16,18,36]. Such behavior is attributed to the planar alignment of bacterial bodies, anisotropic viscosity, and the reduction of the elastic energy required for these bacteria to move along the director field. We track the trajectories of acoustic bubble microswimmers in nematic LC media and collect data on particle velocity, the orientation of the local nematic field, and the order parameter (see Fig. 2a,b). Within our system, we find that the majority of the bubble microswimmers tend to swim parallel to the local director field, similar to bacterial systems. However, a significant amount of the swimmers often move at an angle or even perpendicular to the local director in sharp contrast to bacterial swimmers. The probability distribution of particle orientation with respect to the local nematic field (α_{nV}) reveal bimodal distribution with two well defined and separated peaks at $\alpha_{nV}=0$ and $\alpha_{nV}=\pi/2$, see Fig. 2c. The mode of swimming is not fixed and the same swimmer may swim along or on angle to the director field at different times within one trajectory (see Fig. 2a and Movie 2).

The ability to swim perpendicular to the director field may be attributed to several factors. First, while the aspect ratio of a rod-shaped bubble microswimmer used in our experiments is similar to that of bacteria, the bubble swimmer is significantly larger than a typical bacterium, both in length and diameter (15 μm $\times$ 5 μm vs 2-5 μm $\times \approx$ 0.5-0.7 μm). The larger size of a swimmer reduces the effective anisotropy of the rotational diffusion felt by the swimmer in LC. Second, the self-propulsion mechanism is different and produces much stronger flows than those from bacteria. Bacteria are propelled by a rotating bundle of helical flagella. Orientation of flagella, which are several microns in length and only 20 nm in diameter, is highly sensitive to the local nematic order[37] and can produce thrusts only along the axis of rotation of the bundle that usually reorients along the local director field[38]. In contrast, the position of the air/bubble interface is fixed relative to the swimmer body and the air bubble oscillation can, in principle, produce streaming flows that are redirected by local anisotropy in LC media. These flows may stabilize the swimming direction of a perpendicular swimmer (see Fig. S1 and SI for more details).

A histogram of the swimming velocities V with relative orientation α_{nV} is shown in Fig. 2c, and indicates that the swimmers

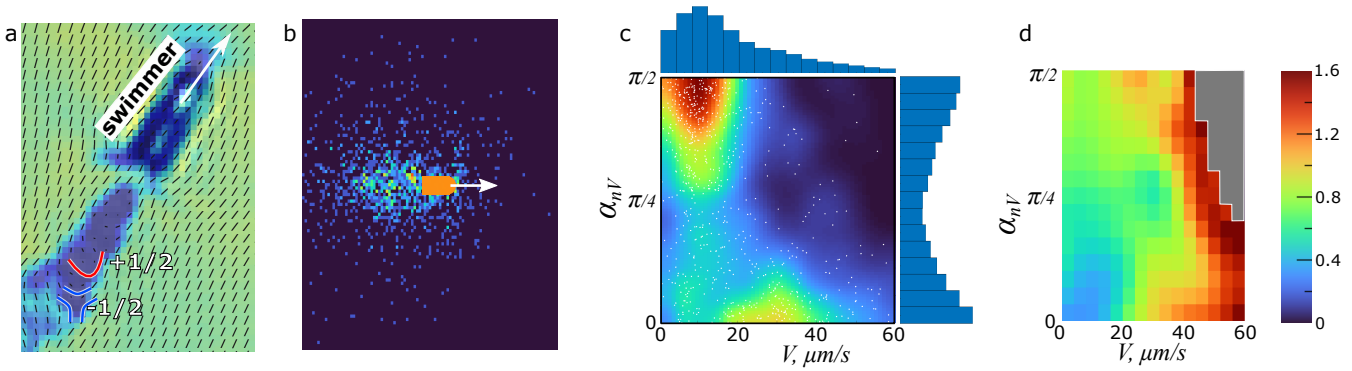

Fig. 3 Topological defects generated by bubble swimmers. (a) A pair of topological defects with charges of +1/2 and -1/2 generated at the tail of a swimmer and schematically indicated by red and blue symbols correspondingly. The direction of the swimmer's velocity is shown by a white arrow. (b) Spatial distribution of generated defects (at the moment of emergence) relative to the orientation of the swimmer. The direction of swimming is indicated by a white arrow. The length of the swimmer is 15 μm. (c) 2D histogram of the velocity V and the orientation angle α_{nV} of the bubble swimmer at the moment of generation of a topological defects pair. Top and right bar plots shows 1D distributions of V and α_{nV} correspondingly. The total number of defects observations (number of white dots in the graph) is 920. (d) Defects generation rate for a swimmer with given velocity V and orientation α_{nV} in units of average number of defect pairs generated by a swimmer per second. The gray area does not contain enough observations due to the extremely low probability of swimmer realizations with such speed V and angle α_{nV}.

are able to move at much higher velocities when oriented parallel to the director field ($\alpha_{nV} = 0$) as compared to the second stable state of $\alpha_{nV} = \pi/2$. As can be seen from Fig. 2 a,b, and Movie 2, a swimmer oriented at $\alpha_{nV} = 81^0$ moves with the speed of 3.8 μm/s, while the same swimmer at $\alpha_{nV} = 4^0$ achieves the velocity of 30 μm/s, a nearly eight-fold increase. Generally, we find the velocities of perpendicular and parallel swimmers are in the range of 0-20 μm/s and 10-40 μm/s respectively (Fig. 2) c. A map of the optical retardance shows that the effective birefringence is significantly reduced near the swimmer as compared to the uniform nematic field in the surrounding areas for both perpendicular and parallel swimmers(Fig.2 a,b) suggestive of a local melting of the LC nematic order near the acoustic bubble swimmers. The swimmers leave a trail of the melted areas along the path of their trajectory (dark blue trail in Fig.2b indicative of suppressed nematic order parameter). Interestingly, we find that for the perpendicular swimmer, the melted region behind the swimmer has a characteristic 'V' shape, see Fig. 2a. This observation provides indirect experimental support for the plausibility of the orientational stabilization mechanism of perpendicular swimmers discussed above (see also Fig. S1).

2.2 Generation of topological defects by the acoustic swimmers

Another feature of the bubble swimmers in the LC media is the ability to generate topological defects. Topological defects are singularities of the director field and are characterized by a topological charge[39,40]. The spontaneous generation and annihilation of topological defects are frequently observed in active nematics[2,41–47]. The bubble swimmer introduces microscopic stress by a hydrodynamic streaming flow generated by the oscillating air bubble and by mechanical motion of the swimmer body. The position of generated defects relative to the swimmer body is shown in Fig.3a. Most defects emerge at the tail of the swimmer, where the hydrodynamic flows are the strongest.

The statistic of defects generation by swimmers of different orientations α_{nV} and the swimming speed V is shown in Fig.3c. Most defects are generated by slow (5-10 umm/s) swimmers moving perpendicular to the director field. To obtain the generation rate as a function of V and α_{nV} we normalize (divide) the obtained defects statistic by PDF shown in Fig. 2c. The result is presented in Fig.3d. As one can expect, the defect generation rate increases with the swimmer velocity V at any orientational angle. That observation is in agreement with previously obtained results that in active nematics the defects number grows with the Ericksen number (Er), a measure of activity in viscoelastic nematic liquid that is proportional to a typical fluid velocity[46]. The defect generation rate strongly depends on the relative orientation of the swimmers. For instance, for $V = 10$ μm/s, the swimmer moving perpendicular to the director field generates on average ≈ 0.8 defect pairs per second, while the swimmer moving parallel to the director field induces only ≈ 0.3 pairs per second. Additionally, we find that acoustic swimmers interact with existing topological defects in the nematic field and their trajectories are scattered upon these interactions (see Fig. S2 and SI for more details. Also see Movies 5, 6, 7).

2.3 Dynamics of "backward" swimmers

A small fraction of the bubble streaming particles in our system (usually < 5%) exhibits unconventional swimming behavior - particles tend to swim towards their open end, where an air bubble is located. Their velocities are comparable to those of the forward swimmers and can similarly be controlled by the strength of the applied acoustic field. Backward swimming has recently been reported in acoustic bubble streaming swimmers in isotropic liquids and has been shown to be associated with the location where the air-fluid interface is pinned in the cylindrical microstructure[32]. When the interface is pinned such that the air-fluid interface protrudes slightly outside the tube opening, the microstreaming flows have been shown to lead inwards towards

the bubble resulting in backward propulsion.

Similar to the forward swimmers, the backward swimmers melt the surrounding liquid crystal as indicated by the areas of lower optical retardance, see Fig. 4. However, the shape of the melted region is quite distinct when compared to the forward swimmer. Whereas the forward swimmers leave a narrow melted "tail" behind along their trajectories, the backward swimmers leave two trails on both sides of the swimmer and create a disclination line along their trajectory (Fig. 4c). Backward swimmers also generate defects near the pulsating bubble similar to the forward swimmers as shown in Fig 4. Nevertheless, while in the case of forward swimmers, the defects quickly annihilate once the swimmer leaves the surrounding area, the backward swimmers usually transport the defects to larger distances by pushing them ahead of the swimmer (see Fig 4a-c and Movie 4).

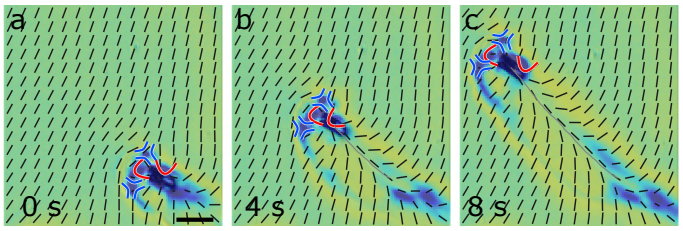

Fig. 4 Backward swimmer. (a-c) Director field and topological defects around a backward swimmer moving perpendicular to the local director field. The flow created by the oscillating air bubble melts LC ahead of the swimmer and generates two pairs of defects that are pushed by the swimmer along the trajectory. The trajectory of the swimmer is shown by a gray line. Also, see Movie 4.

3 Conclusions

We have demonstrated the ability of the air-bubble streaming microstructures to efficiently propel in an anisotropic viscous medium of nematic LC upon application of an ultrasonic acoustic field. In contrast to biological live swimmers, synthetic acoustic swimmers offer a new degree of control over the swimming activity and enable fast on/off switching of the activity on demand. Acoustically streaming swimmers in LC exhibit a bistable state where the swimmers either propel along the local nematic field or swim perpendicular to it. The swimming speed along the local director field though is significantly higher than perpendicular to it. In both cases, swimming particles continuously generate topological defects in the nematic liquid crystals. The majority of the defects are induced near the pulsating air-bubble, and the defect generation rate is proportional to the swimmer's velocity and also strongly depends on the orientation of the swimmer's velocity with respect to the local director field. The air-bubble streaming swimmers represent a promising approach for the design of fully synthetic active liquid crystalline materials with a microscopically tunable activity delivered by the swimmers powered by acoustic fields.

4 Methods

4.1 Fabrication of the bubble-based microswimmers

The cylindrical microstructures were fabricated using a two-photon polymerization based on a 3D lithography system (Nanoscribe GmbH, Germany). A high-resolution photoresist (IP-Dip) was used to fabricate around 20000 structures on an ITO-coated silica substrate in ≈ 7 hours. After the lithography step, the sample was developed in PGMEA solution for 30 minutes and then rinsed with IPA to wash off the excess developer. To successfully trap air bubbles in the capsules, the sample was incubated in Trichlorododecylsilane vapor at 70°C for 30 min and allowed to rest for 24 hours at room temperature to form a hydrophobic monolayer. The sample was placed in air plasma to activate the surface for 10 minutes before the surface treatment. Finally, the completed capsules were scratched off the substrate by using a pipette tip and transferred to the fluidic chamber.

4.2 Experimental setup

The experimental chamber was prepared by sandwiching two glass slides with 5 um tracer particles as spacers. A droplet of a suspension of 12 wt% chromonic lyotropic LC material disodium cromoglycate (DSCG) and the hydrophobic microstructures was placed between the two glass slides. The concentration of the LC material was chosen such that the LC is nematic at room temperature with a low viscosity. A piezoceramic transducer (1 MHz; STEMiNC Inc.) was glued to the bottom glass slide using a 2 component glue that ensures an effective transmission of the acoustic field into the experimental chamber. A typical frequency range of 900 kHz to 1.3 MHz and a voltage range of 8 to 20 V were used to ensure the streaming of the bubbles in the microstructures.

Conflicts of interest

There is no conflict of interest.

Acknowledgements

The research was supported by the U.S. Department of Energy, Office of Science, Basic Energy Sciences, Materials Sciences and Engineering Division. Use of the Center for Nanoscale Materials, an Office of Science user facility, was supported by the U.S. Department of Energy, Office of Science, Office of Basic Energy Sciences, under Contract No. DE-AC02-06CH11357.

Notes and references

1 S. Ramaswamy, *Annual Review of Condensed Matter Physics*, 2010, **1**, 323–345.
2 T. Sanchez, D. T. Chen, S. J. DeCamp, M. Heymann and Z. Dogic, *Nature*, 2012, **491**, 431–434.
3 A. Snezhko, *Current opinion in colloid & interface science*, 2016, **21**, 65–75.
4 I. S. Aranson, *Physics-Uspekhi*, 2013, **56**, 79.
5 C. Bechinger, R. Di Leonardo, H. Löwen, C. Reichhardt, G. Volpe and G. Volpe, *Reviews of Modern Physics*, 2016, **88**, 045006.

6 A. Zöttl and H. Stark, *Journal of Physics: Condensed Matter*, 2016, **28**, 253001.

7 J. E. Martin and A. Snezhko, *Reports on Progress in Physics*, 2013, **76**, 126601.

8 P.-G. De Gennes and J. Prost, *The physics of liquid crystals*, Oxford university press, 1993.

9 I. Muševič, M. Škarabot, U. Tkalec, M. Ravnik and S. Žumer, *Science*, 2006, **313**, 954–958.

10 A. Doostmohammadi, J. Ignés-Mullol, J. M. Yeomans and F. Sagués, *Nature communications*, 2018, **9**, 1–13.

11 R. Zhang, A. Mozaffari and J. J. de Pablo, *Nature Reviews Materials*, 2021, **6**, 437–453.

12 G. Duclos, R. Adkins, D. Banerjee, M. S. Peterson, M. Varghese, I. Kolvin, A. Baskaran, R. A. Pelcovits, T. R. Powers, A. Baskaran *et al.*, *Science*, 2020, **367**, 1120–1124.

13 V. Schaller, C. Weber, C. Semmrich, E. Frey and A. R. Bausch, *Nature*, 2010, **467**, 73–77.

14 R. Mueller, J. M. Yeomans and A. Doostmohammadi, *Physical review letters*, 2019, **122**, 048004.

15 C. J. Woolverton, E. Gustely, L. Li and O. D. Lavrentovich, *Liquid crystals*, 2005, **32**, 417–423.

16 S. Zhou, A. Sokolov, O. D. Lavrentovich and I. S. Aranson, *Proceedings of the National Academy of Sciences*, 2014, **111**, 1265–1270.

17 A. Sokolov, S. Zhou, O. D. Lavrentovich and I. S. Aranson, *Physical Review E*, 2015, **91**, 013009.

18 P. C. Mushenheim, R. R. Trivedi, H. H. Tuson, D. B. Weibel and N. L. Abbott, *Soft Matter*, 2014, **10**, 88–95.

19 M. M. Genkin, A. Sokolov, O. D. Lavrentovich and I. S. Aranson, *Physical Review X*, 2017, **7**, 011029.

20 A. Sokolov, A. Mozaffari, R. Zhang, J. J. De Pablo and A. Snezhko, *Physical Review X*, 2019, **9**, 031014.

21 S. Sanchez, L. Soler and J. Katuri, *Angewandte Chemie International Edition*, 2015, **54**, 1414–1444.

22 T. Yao, Ž. Kos, Q. X. Zhang, Y. Luo, E. B. Steager, M. Ravnik and K. J. Stebe, *Science Advances*, 2022, **8**, eabn8176.

23 D. Ahmed, M. Lu, A. Nourhani, P. E. Lammert, Z. Stratton, H. S. Muddana, V. H. Crespi and T. J. Huang, *Scientific reports*, 2015, **5**, 1–8.

24 J. Feng, J. Yuan and S. K. Cho, *Lab on a Chip*, 2016, **16**, 2317–2325.

25 J. Feng, J. Yuan and S. K. Cho, *Lab on a Chip*, 2015, **15**, 1554–1562.

26 L. Ren, N. Nama, J. M. McNeill, F. Soto, Z. Yan, W. Liu, W. Wang, J. Wang and T. E. Mallouk, *Science Advances*, 2019, **5**, eaax3084.

27 A. Aghakhani, O. Yasa, P. Wrede and M. Sitti, *Proceedings of the National Academy of Sciences*, 2020, **117**, 3469–3477.

28 J. M. McNeill, N. Nama, J. M. Braxton and T. E. Mallouk, *ACS Nano*, 2020, **14**, 7520–7528.

29 D. Gottlieb and O. Arteaga, *Optics Express*, 2021, **29**, 34723–34734.

30 R. Dijkink, J. Van Der Dennen, C. Ohl and A. Prosperetti, *Journal of micromechanics and microengineering*, 2006, **16**, 1653.

31 D. Ahmed, C. Dillinger, A. Hong and B. J. Nelson, *Advanced Materials Technologies*, 2017, **2**, 1700050.

32 F.-W. Liu, Y. Zhan and S. K. Cho, *Journal of Micromechanics and Microengineering*, 2021, **31**, 084001.

33 M. Mullen, B. Lüthi and M. Stephen, *Physical Review Letters*, 1972, **28**, 799.

34 E. Pereira, S. Fumeron and F. Moraes, *Physical Review E*, 2013, **87**, 022506.

35 K. Miyano and J. Ketterson, *Physical acoustics*, Elsevier, 1979, vol. 14, pp. 93–178.

36 A. Kumar, T. Galstian, S. K. Pattanayek and S. Rainville, *Molecular Crystals and Liquid Crystals*, 2013, **574**, 33–39.

37 M. Goral, E. Clement, T. Darnige, T. Lopez-Leon and A. Lindner, *arXiv preprint arXiv:2206.10316*, 2022.

38 S. Zhou, O. Tovkach, D. Golovaty, A. Sokolov, I. S. Aranson and O. D. Lavrentovich, *New Journal of Physics*, 2017, **19**, 055006.

39 M. Kleman and O. D. Lavrentovich, *Soft matter physics: an introduction*, Springer, 2003.

40 P. De Gennes and J. Prost, *Press New York*, 1995.

41 V. Narayan, S. Ramaswamy and N. Menon, *Science*, 2007, **317**, 105–108.

42 F. C. Keber, E. Loiseau, T. Sanchez, S. J. DeCamp, L. Giomi, M. J. Bowick, M. C. Marchetti, Z. Dogic and A. R. Bausch, *Science*, 2014, **345**, 1135–1139.

43 S. J. DeCamp, G. S. Redner, A. Baskaran, M. F. Hagan and Z. Dogic, *Nature materials*, 2015, **14**, 1110–1115.

44 A. U. Oza and J. Dunkel, *New Journal of Physics*, 2016, **18**, 093006.

45 S. P. Thampi, R. Golestanian and J. M. Yeomans, *EPL (Europhysics Letters)*, 2014, **105**, 18001.

46 L. Giomi, M. J. Bowick, P. Mishra, R. Sknepnek and M. Cristina Marchetti, *Philosophical Transactions of the Royal Society A: Mathematical, Physical and Engineering Sciences*, 2014, **372**, 20130365.

47 I. S. Aranson, *Physics-Uspekhi*, 2019, **62**, 892.